EVALUATION OF COMPONENT MODE SYNTHESIS METHODS FOR THE DETECTION OF MODAL INTERACTION THROUGH ROTOR STATOR CONTACTS

A. Batailly, GeM, École Centrale de Nantes, France
M. Legrand, Laboratoire de dynamique des structures et vibrations, Université McGill, Québec
P. Cartraud, GeM, École Centrale de Nantes, France
C. Pierre, Laboratoire de dynamique des structures et vibrations, Université McGill, Québec
J.-P. Lombard, Snecma, Site de Villaroche, France

Cet article fait partie des actes de la conférence ASME DETC 2009

Abstract

The study of interactions through direct contact between blade-tips and outer casings in modern turbomachines may be very time-consuming when the classical finite element method is used. The construction of reduced-order models using component mode synthesis (CMS) methods generally allows for dramatic increase in computational efficiency and may be used in order to improve the knowledge over these interaction phenomena. Among the available approaches, both a fixed-interface method and a free-interface method are considered here in an original manner to reduce the size of a realistic two-dimensional model. The equations of motion are solved using an explicit time integration scheme with the Lagrange multiplier method where friction is accounted for. This method offers energy momentum conserving which is a critical point to ensure the convergence of the algorithm. Moreover, it is shown that even in a non-linear framework the reduced-order models converge to the finite element solution as the number of modes included in the models increases. Considering the fixed-interface method of Craig-Bampton (CB) and the free-interface method of Craig-Chang-Martinez (CCM), it is shown that a method with fast displacement convergence may be less efficient in terms of motion convergence.

Nomenclature

β	Angle between two blades
$\mathbf{F}$	Force vector
$\mathbf{K}$	Stiffness matrix

$\mathbf{M}$	Mass matrix
$\mathbf{q}$	Degrees of freedom vector
η	Craig-Bampton (CB) reduction parameter: number of fixed-interface modes kept in the reduced model.
μ	Friction coefficient
Ω	Angular velocity of the bladed disk
$\omega_{\mathrm{c}}(k)$	Critical angular velocity for a k-nodal diameter load
ϕ	Craig-Chang-Martinez (CCM) reduction parameter: number of normal modes kept in the reduced model.
Φ_{CB}	Craig-Bampton (CB) transformation matrix
$_{\mathrm{B}}$	Subscript referring to boundary dof
$_{\mathrm{I}}$	Subscript referring to internal dof
f_{b}	Eigenfrequency of the bladed disk
f_{c}	Eigenfrequency of the casing
h	Time step
n_{d}	Number of nodal diameters
u_{fe}	Finite element reference solution

1 Introduction

In modern turbomachines such as aircraft jet engines, structural contacts between the casing and the bladed disk can initiate nonlinear vibrations that can be responsible for severe damages. The power of such engines can be increased by reducing the clearance between the blade tips and the casing. Unfortunately, this may lead to more frequent contacts between the two components.

In this study, we focus on a specific kind of interaction, commonly named "modal interaction". Previous theoretical studies [1, 2, 3] have been achieved on these interactions (experimental results are also presented in [3]) that can arise for cyclic and axi-symmetric structures under certain conditions:

1. both structures (bladed disk and casing) must vibrate over a vibration mode with the same number of nodal diameters.

2. both structures must vibrate at the eigenfrequency of the mode of interest.

3. the rotating modes of the bladed disk may travel at the same absolute speed as the forward rotating mode in the casing.

These three conditions can be summarized as [4]:

$$f_c = \frac{n_d \Omega}{2\pi} - f_b \tag{1}$$

with f_c eigenfrequency of the casing, f_b eigenfrequency of the bladed disk, n_d number of diameters of the associated vibration modes and Ω angular velocity of the bladed disk. Equation (1) allows us to define critical speeds for each configuration of bladed disk and casing.

The point of present work is to analyze modal interaction using 2D planar models with the use of component mode synthesis (CMS) methods. Such methods are required in order to reduce computation time. Among the very large number of available CMS methods [5, 6, 7, 8] only the ones compatible with contact algorithms may be considered. Indeed, treatment of contact forces and correction of displacements on certain degrees of freedom (dof) implies to keep these dof in the reduced system to avoid backward and forward between the reduced-order model and the full finite element model that would be dreadfully time consuming. Considering that most of the CMS methods lead to a reduced order model governed by modal dof with no explicit physical meaning, only a few methods are actually eligible for this study. The Craig-Bampton (CB) method [6] and the Craig-Chang-Martinez (CCM) method [9] are the most popular methods that match our criteria. The objective of this study is to evaluate the sensitivity of modal interaction detection toward the CMS method used.

The convergence of CMS methods toward the finite element solution is analyzed in terms of *displacement convergence* or *motion convergence*. Displacement convergence refers to the convergence of the displacement field while motion convergence refers to the convergence in terms of type of motions detected and interaction between the casing and the bladed disk.

2 Modeling

The 2D finite element models of the bladed disk and the casing are now presented. The model allows both normal contact and friction forces treatment (friction coefficient is set to $\mu = 0.2$) between the casing and the tip of the blades. Both casing and bladed disk models are introduced in [10].

Bladed disk

The bladed disk, as depicted in Fig. 1, is composed of 22 blades and its description is similar to the one used in [2]. In many studies about bladed disks

blades are modeled using pretwisted tapered beams [11, 12, 13]. However, we focus on contact treatment on the tip of the blades and the application of CMS methods combined with the contact algorithm which leads to considering simpler modeling. That is why each blade is discretized with the usual Euler-Bernoulli straight beams. The global curvature of the blade is achieved through an angle a_{i} between finite elements. The inter blade phase angle is denoted by $\beta = \frac{2\pi}{22}$. The total number of dof for the bladed disk in this study is 748. In the flexural direction v, the local shape functions are:

$$\begin{aligned} N_1(s) &= 1 - 2s^2 + 2s^3;\ N_2(s) = l_{\mathrm{b}}(s - 2s^2 + s^3) \\ N_3(s) &= 3s^2 - 2s^3;\ N_4(s) = l_{\mathrm{b}}(-s^2 + s^3) \end{aligned} \tag{2}$$

while they are linear along the axial displacement u:

$$M_1(s) = 1 - s;\ M_2(s) = s,\ s\ \in\ [0, 1] \tag{3}$$

The discretized displacement field of element i whose nodes are denoted i and $i+1$ is written as:

$$\begin{aligned} v_{\mathrm{r}}^{\mathrm{i}}(s) &= N_1(s)v_{\mathrm{r}}^{\mathrm{i}} + N_2(s)\theta_{\mathrm{r}}^{\mathrm{i}} + N_3(s)v_{\mathrm{r}}^{\mathrm{i+1}} + N_4(s)\theta_{\mathrm{r}}^{\mathrm{i+1}} \\ \theta_{\mathrm{r}}^{\mathrm{i}}(s) &= N_{1,s}(s)v_{\mathrm{r}}^{\mathrm{i}} + N_{2,s}(s)\theta_{\mathrm{r}}^{\mathrm{i}} + N_{3,s}(s)v_{\mathrm{r}}^{\mathrm{i+1}} + N_{4,s}(s)\theta_{\mathrm{r}}^{\mathrm{i+1}} \\ u_{\mathrm{r}}^{\mathrm{i}}(s) &= M_1(s)u_{\mathrm{r}}^{\mathrm{i}} + M_2(s)u_{\mathrm{r}}^{\mathrm{i+1}} \end{aligned} \tag{4}$$

Casing

The casing is modeled as a ring and is discretized using two-noded curved beam finite elements, as pictured in Fig. 1. There are 40 curved beam finite element around the casing, with a total number of 160 dof.

A polar coordinate system with unit vectors $e_{\mathrm{r_c}}$ and $e_{\theta_{\mathrm{c}}}$ is assigned to the casing. The finite element description involves four dof per node: u_{c}, $u_{\mathrm{c,s}}$, v_{c} and $v_{\mathrm{c,s}}$. The initial location of node i is given by the doublet (R_{c},$\theta_{\mathrm{c}}^{\mathrm{i}}$), R_{c} stands for the radius of the casing and l_{c} the length of the element. The shape functions are similar to those of the bladed disk, by replacing x by s and l_{b} by the length l_{c} of a finite element of the casing in Eq. (2) where $s \in$ [0,1] is the local path variable. This formulation is taken from [14] where it is shown that such finite element are locking free. The discretized displacement field of element i whose nodes are denoted i and $i+1$ is written as:

$$\begin{aligned} u_{\mathrm{c}}^{\mathrm{i}}(s) &= N_1(s)u_{\mathrm{c(n)}}^{\mathrm{i}} + N_2(s)u_{\mathrm{c(n),s}}^{\mathrm{i}} + N_3(s)u_{\mathrm{c(n)}}^{\mathrm{i+1}} + N_4(s)u_{\mathrm{c(n),s}}^{\mathrm{i+1}} \\ v_{\mathrm{c}}^{\mathrm{i}}(s) &= N_1(s)v_{\mathrm{c(n)}}^{\mathrm{i}} + N_2(s)v_{\mathrm{c(n),s}}^{\mathrm{i}} + N_3(s)v_{\mathrm{c(n)}}^{\mathrm{i+1}} + N_4(s)v_{\mathrm{c(n),s}}^{\mathrm{i+1}} \end{aligned} \tag{5}$$

Characteristics of the model

Table 1 summarizes the mechanical properties of the model, that match certain criteria such as the fact that the eigenfrequencies of the casing are larger than those of the bladed disk.

	Casing	Bladed disk
Y.Modulus	$E_c = 2.8 \cdot 10^3$	$E_b = 8.3 \cdot 10^6$
mass	$\rho_c = 2800$	$\rho_b = 7800$
thickness	$h_c = 5$	$h_b = 5$
width	$w_c = 50$	$w_b = 50$
radius	$R_c = 250.5$	$R_b = 250$
d.o.f	$n_c = 160$	$n_b = 748$
modal damping	$\xi_c = 0.03$	$\xi_b = 0.005$
number of blades		$N = 22$

Table 1 – Characteristics of the model

3 Solution method

Time integration

The numerical methods are introduced in this section and described in the general framework of the finite element methods. This part is devoted to the computation of the reference solution. The general problem to be solved may be written as:

$$\begin{aligned} &\mathbf{M}\ddot{\mathbf{q}} + \mathbf{D}\dot{\mathbf{q}} + \mathbf{K}\mathbf{q} = \mathbf{F} \\ &\mathbf{q}(t = t_0) = \mathbf{q}_0 \\ &\dot{\mathbf{q}}(t = t_0) = \dot{\mathbf{q}}_0 \end{aligned} \tag{6}$$

The contact conditions, referred to as the Kuhn-Tucker optimality conditions take the form:

$$\forall \mathbf{x} \in \Gamma_c^m,\ \mathbf{t_N} \geq 0,\ g \geq 0,\ \mathbf{t_N} g = 0 \tag{7}$$

where Γ_c^m is the master surface (bladed disk) and $\mathbf{t_N}$ stands for the contact pressure, assumed positive, acting on the slave surface Γ_c^s (casing). This problem is solved using the explicit central differences scheme together with the forward increment Lagrangian method [15, 16] and more details about the algorithm used in this work may be found in [2].

Component mode synthesis

In most industrial applications, very large finite element models lead to cumbersome computation times. One way to reduce these computation times relies in the use of component mode synthesis procedures [10]. Many studies of these CMS methods have been carried out by coupling them to substructuring approaches [5]. Only the modal reduction aspect is considered here: CB method is applied on the bladed disk and on the casing considering each of them as on substructure. The interface dof are related to each other in a strongly nonlinear fashion through unilateral contact and friction conditions.

CB and CCM methods first require the distinction of the dof of the structure within two groups: the internal dof and the boundary dof. In

general the definition of these groups is closely related to the loadings applied on the structures. In this study the boundary is supposed to contain all the dof that might be supporting any contact force during the interaction, meaning the two dof u and v at the tip of each blade[1] for the bladed disk and the u and v dof for each node of the casing.

Application

A reorganization of Eq. (6) is necessary, separating the dof in two groups: the internal dof ($\mathbf{q}_{\mathrm{I}}$) and the interface ($\mathbf{q}_{\mathrm{B}}$) yielding:

$$\begin{bmatrix} \mathbf{M}_{\mathrm{II}} & \mathbf{M}_{\mathrm{BI}} \\ \mathbf{M}_{\mathrm{IB}} & \mathbf{M}_{\mathrm{BB}} \end{bmatrix} \begin{pmatrix} \ddot{\mathbf{q}}_{\mathrm{I}} \\ \ddot{\mathbf{q}}_{\mathrm{B}} \end{pmatrix} + \begin{bmatrix} \mathbf{D}_{\mathrm{II}} & \mathbf{D}_{\mathrm{BI}} \\ \mathbf{D}_{\mathrm{IB}} & \mathbf{D}_{\mathrm{BB}} \end{bmatrix} \begin{pmatrix} \dot{\mathbf{q}}_{\mathrm{I}} \\ \dot{\mathbf{q}}_{\mathrm{B}} \end{pmatrix} + \begin{bmatrix} \mathbf{K}_{\mathrm{II}} & \mathbf{K}_{\mathrm{BI}} \\ \mathbf{K}_{\mathrm{IB}} & \mathbf{K}_{\mathrm{BB}} \end{bmatrix} \begin{pmatrix} \mathbf{q}_{\mathrm{I}} \\ \mathbf{q}_{\mathrm{B}} \end{pmatrix} = \begin{pmatrix} \mathbf{F}_{\mathrm{I}} \\ \mathbf{F}_{\mathrm{B}} \end{pmatrix} \tag{8}$$

Applying a CMS method consists in finding a reduction basis which dimension is smaller than the number of dof of the structure reduced. This basis is represented through a rectangular matrix Φ. This matrix is defined by the choice of the CMS technique.

Craig-Bampton method

The reduction basis of the CB method is composed of the following modes [6, 10]:

1. fixed interface modes: Φ_{fix}
2. constraint modes: Φ_{cons}

The reduction matrix of the Craig Bampton method Φ_{CB} is:

$$\Phi_{\mathrm{CB}} = [\Phi_{\mathrm{fix}} \Phi_{\mathrm{cons}}] \tag{9}$$

The number of fixed-interface modes η kept in the reduction basis is the parameter of reduction:

$$\begin{pmatrix} \mathbf{q}_{\mathrm{I}} \\ \mathbf{q}_{\mathrm{B}} \end{pmatrix} = \Phi_{\mathrm{CB}} \begin{pmatrix} \mathbf{u}_{\eta} \\ \mathbf{q}_{\mathrm{B}} \end{pmatrix} \tag{10}$$

The projection of the equations of motion in the reduced space consists in the following operations[2]:

$$\hat{\mathbf{K}} = \Phi_{\mathrm{CB}}^{\mathrm{T}} \mathbf{K} \Phi_{\mathrm{CB}} \quad \text{and} \quad \hat{\mathbf{M}} = \Phi_{\mathrm{CB}}^{\mathrm{T}} \mathbf{M} \Phi_{\mathrm{CB}} \tag{11}$$

[1] Rotational θ on the tip of the blades is also considered as part of the boundary in the case of the CCM method in order to enrich the space of the attachment modes. This does not modify contact treatment.

[2] Damping matrix $\hat{\mathbf{D}}$ is usually computed directly from reduced stiffness and mass matrices $\hat{\mathbf{K}}$ and $\hat{\mathbf{M}}$

Consequently, the dynamic equation in the reduced-order space becomes:

$$\begin{bmatrix} \hat{\mathbf{M}}_{\eta\eta} & \hat{\mathbf{M}}_{\mathrm{B}\eta} \\ \hat{\mathbf{M}}_{\eta\mathrm{B}} & \hat{\mathbf{M}}_{\mathrm{BB}} \end{bmatrix} \begin{pmatrix} \ddot{\mathbf{u}}_\eta \\ \ddot{\mathbf{q}}_\mathrm{B} \end{pmatrix} + \begin{bmatrix} \hat{\mathbf{D}}_{\eta\eta} & \hat{\mathbf{D}}_{\mathrm{B}\eta} \\ \hat{\mathbf{D}}_{\eta\mathrm{B}} & \hat{\mathbf{D}}_{\mathrm{BB}} \end{bmatrix} \begin{pmatrix} \dot{\mathbf{u}}_\eta \\ \dot{\mathbf{q}}_\mathrm{B} \end{pmatrix} + \begin{bmatrix} \hat{\mathbf{K}}_{\eta\eta} & \hat{\mathbf{K}}_{\mathrm{B}\eta} \\ \hat{\mathbf{K}}_{\eta\mathrm{B}} & \hat{\mathbf{K}}_{\mathrm{BB}} \end{bmatrix} \begin{pmatrix} \mathbf{u}_\eta \\ \mathbf{q}_\mathrm{B} \end{pmatrix} = \begin{pmatrix} \mathbf{F}_\eta \\ \mathbf{F}_\mathrm{B} \end{pmatrix} \tag{12}$$

Craig-Chang-Martinez method

This method is an enriched Craig-Martinez method [8, 17]. The reduction basis is composed of the following modes [18, 10]:

1. free vibration modes
2. attachment modes

From a theoretical point of view, there is no restriction in the choice of these modes. From Eq. (6), the projection of the displacements $\mathbf{q}$ onto the modal coordinates leads to:

$$\mathbf{q} = \Phi_1 \mathbf{u}_1 + \Phi_2 \mathbf{u}_2 \tag{13}$$

where Φ_1 represents the free vibration modes kept in the reduction basis and Φ_2 the modes that will be discarded for the reduction (high frequency modes).

Considering the following approximation:

$$\forall\, \omega_2^2 \in \mathrm{diag}(\Omega_2), \omega^2 \ll \omega_2^2 \Rightarrow \Omega_2 \mathbf{u}_2 = \Phi_2^\mathrm{T} \mathbf{F} \tag{14}$$

and using the notation $\mathbf{R} = \mathbf{K}^{-1} - \Phi_1 \Omega_1^{-1} \Phi_1^\mathrm{T}$, the projection introduced in Eq. (13) can be written as:

$$\mathbf{q} = \Phi_1 \mathbf{u}_1 + \mathbf{R}\mathbf{F} \tag{15}$$

With Eq. (8), $\mathbf{q} = (\mathbf{q}_\mathrm{B}, \mathbf{q}_\mathrm{I})^\mathrm{T}$

$$\begin{pmatrix} \mathbf{q}_\mathrm{B} \\ \mathbf{q}_\mathrm{I} \end{pmatrix} = \begin{bmatrix} \Phi_{1\mathrm{B}} \\ \Phi_{1\mathrm{I}} \end{bmatrix} \mathbf{u}_1 + \begin{bmatrix} \mathbf{R}_\mathrm{B} \\ \mathbf{R}_\mathrm{I} \end{bmatrix} \mathbf{F} \tag{16}$$

This projection leads to the final equation:

$$\begin{pmatrix} \mathbf{q}_\mathrm{B} \\ \mathbf{q}_\mathrm{I} \end{pmatrix} = \underbrace{\begin{bmatrix} \mathbf{I}_{\mathrm{Bf}} & \mathbf{0} \\ \mathbf{R}_\mathrm{I}\mathbf{R}_\mathrm{B}^{-1} & \Phi_{1\mathrm{i}} - \mathbf{R}_\mathrm{I}\mathbf{R}_\mathrm{B}^{-1}\Phi_{1\mathrm{B}} \end{bmatrix}}_{\mathbf{P}_\mathrm{CM}} \begin{pmatrix} \mathbf{q}_\mathrm{B} \\ \mathbf{u}_1 \end{pmatrix} \tag{17}$$

where $\mathbf{P}_\mathrm{CM}$ is defined as the reduction matrix for the Craig-Martinez method. An alternative formulation of the Craig-Martinez method consists in adding attachment modes to the matrix Φ_1 in Eq. (15). This enrichment leads to the CCM method which is used in this paper.

4 Results

Note: *displacements and time have been normalized and no unit is provided in the sequel.*

Convergence analysis

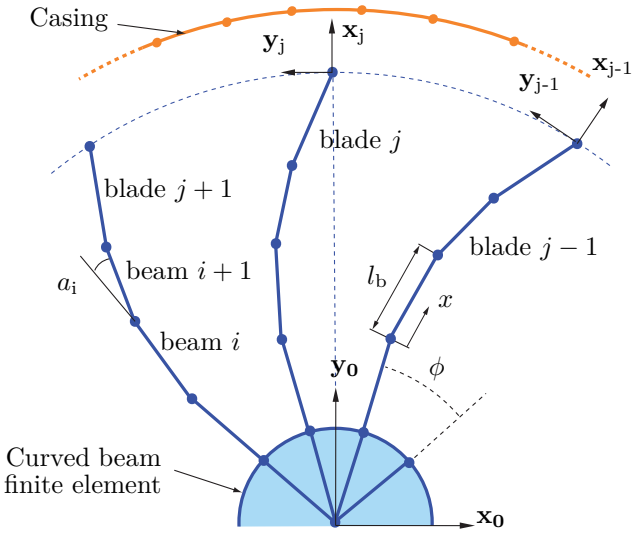

Figure 1 – Two-dimensional model used in the study

The interface of the bladed disk contains 44 dof where contact constraints are treated, namely u and v at the tip of each blade. The casing is not reduced since its contact is managed on every node of the structure. The initial clearance between the tip of the blades and the casing is 1 mm. The rotational velocity of the bladed disk is constant for each simulation. Modal damping is applied for both structures. At time $t = 0$, an external loading is applied on the casing. The deformation of the casing under this loading depends on the n_d parameter: number of nodal diameters of the two free vibration modes on which the kinematic of the casing is reduced. The loading is applied over $t = 2 \cdot 10^{-4}$ s.

With similar conditions, three specific interaction motions were detected in [2] where models were projected in the modal space along two n_d-nodal diameter vibration modes subsequently implying strong kinematic restrictions.

In total, three kinds of motions were observed in [2], namely damped, sustained and divergent motions respectively pictured in Figs. 2(a), 2(b) and 2(c). Among the different sustained motions observed, a specific kind involving locking was detected: a few blades come in permanent contact with the casing, as illustrated in Fig. 2(c), and push a forward rotating mode.

Beside of these three motions, relations have been established between the number of blades and the kind of modal interaction detected. Precisely, it has been noticed that the interaction depends on the divisibility of the number of blades N by the number of diameters n_{d} of the load exerted on the casing. A 3-nodal diameter load on the casing might lead to locked sustained motions with a 30 blades bladed disk while it could only lead to unlocked sustained motions with a 29 blades bladed disk. These results match geometrical observations: a stable interaction configuration can only occur if the geometry of the deformed casing and bladed disk are compatible. It was also noticed that when the geometry allows for the system to be perfectly symmetric in terms of N and n_{d}, the contact points will remain at the same blade tips for all times.

All these considerations are explored in more details with new models in the sequel.

Time convergence

The time step of the explicit central differences scheme is $h = 2.5 \cdot 10^{-7}$ s. This value has been obtained by considering both a convergence study for damped and locked motions, respectively depicted in Figs. 3(a) and 3(b), and the following condition which is classical in linear analysis:

$$h < \frac{2}{\omega_{\max}} = 8.49 \cdot 10^{-7} \text{ s} \tag{18}$$

Both Figs. 3(a) and 3(b) show blade tip/casing distance for a single blade and different time steps. While convergence is easily observed as soon as $h < 10^{-5}$ s in Fig. 3(a), it can be seen that the motion detected in Fig. 3(b) requires a smaller time step and convergence is only reached when $h < 5 \cdot 10^{-7}$ s: this shows that linear condition (18) is not restrictive enough for non-linear systems.

Convergence regarding to the reduction basis

The convergence of reduced-order models constructed with CB and CCM techniques is shown for each of the three interaction motions pictured in Figs. 2(a), 2(b) and 2(c). While damped and locked motions are obtained with $n_{\mathrm{d}} = 2$, the sustained motion is obtained for $n_{\mathrm{d}} = 3$ only. Indeed, it has been notice [2] that locked motions may only be observed when the value of n_{d} divides the number of blades. If not, sustained motion is more likely to occur.

Craig-Bampton method

The convergence of the results for CB reduced-order models when η increases is shown in Figs. 4(a), 4(b) and 4(c)[3]. One may clearly observe the high

[3]Results are shown as blade tip/casing distances for a blade randomly chosen. Results in terms of convergence are similar for other blades.

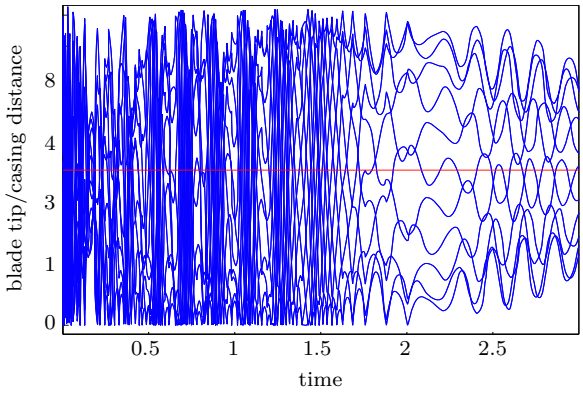

(a) Damped motion: $\Omega = 0.4$, $n_{\mathsf{d}} = 2$

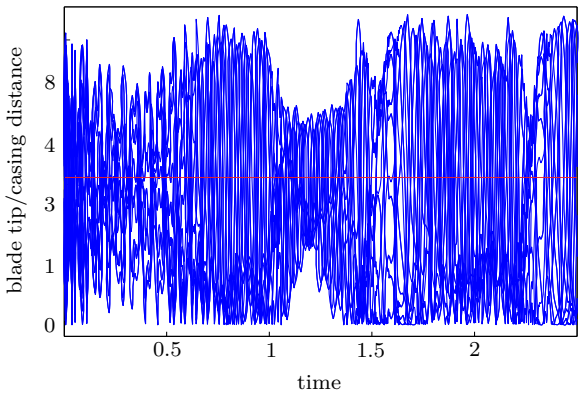

(b) Sustained motion: $\Omega = 1.75$, $n_{\mathsf{d}} = 3$

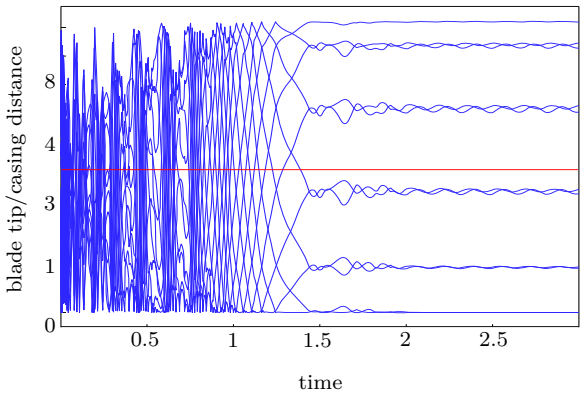

(c) Locked motion: $\Omega = 0.55$, $n_{\mathsf{d}} = 2$

Figure 2 – Blade tip/casing distances, initial clearance (—)

sensitivity of the results to the reduction basis in the case of locked and sustained motions in Figs. 4(b) and 4(c). The quality of the approximation of the blade tip displacements directly depends on the modal reduction basis. As a consequence, the reduction basis will influence the blades that will lock

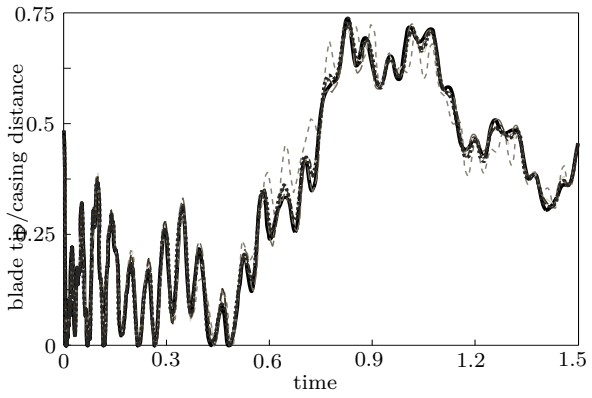

(a) Damped motion, blade 9, $n_{\mathsf{d}} = 3$

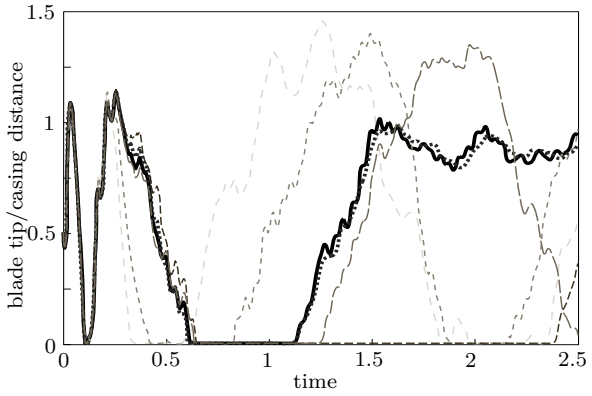

(b) Locked motion, blade 2, $n_{\mathsf{d}} = 2$

Figure 3 – Blade tip/casing distance for two blades and two different simulations when time steps varies: $h = 10^{-5}$ s (——), $h = 5 \cdot 10^{-6}$ s (——), $h = 10^{-6}$ s (——), $h = 5 \cdot 10^{-7}$ s (——), $h = 2.5 \cdot 10^{-7}$ s (▪▪▪▪▪) and $h = 10^{-7}$ s (▬▬)

on the casing. If the locking blades change, then all the displacements on the bladed disk are modified which causes the variation of vibration level observed in Figs. 4(b) and 4(c).

Craig-Chang-Martinez method

Results of the convergence of the reduced-order-models are shown for damped, locked and sustained motions in Fig. 5(a), 5(b) and 5(c), respectively. Differences observed in terms of convergence with the CB method are not significant since convergence seems faster for locked motions and slower for damped motions. However, as previously observed for the CB method, a very high number of modes is required to ensure convergence in terms of blade tip displacements.

Results obtained for the two CMS methods show that the convergence toward the finite element solution is fairly slow. For the CB method, it

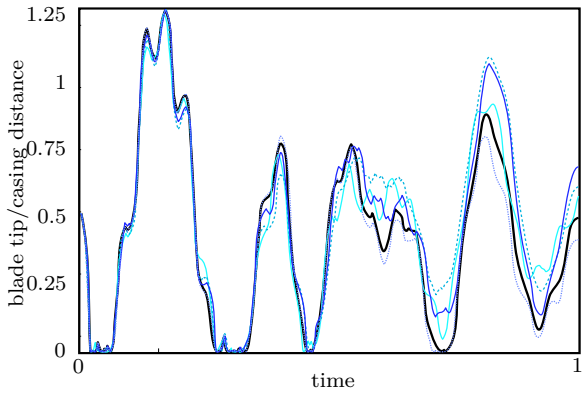

(a) Damped motion, blade 10

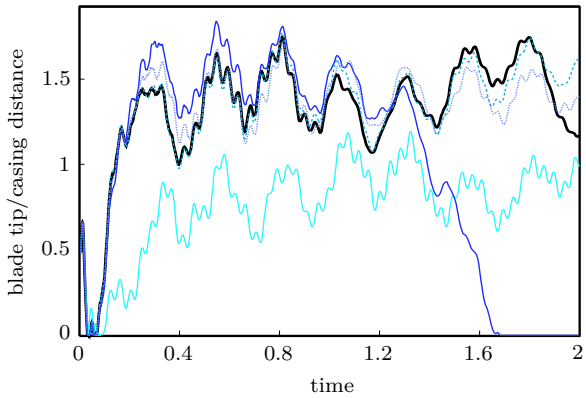

(b) Locked motion, blade 9

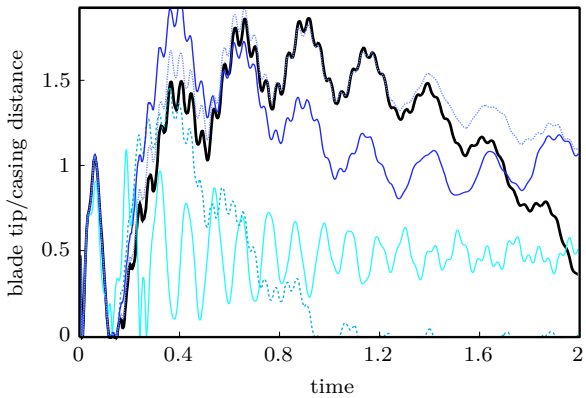

(c) Sustained motion, blade 2

Figure 4 – Convergence of the results obtained with CB method for each kind of interaction $\eta = 0$ (——); $\eta = 44$ (- - -); $\eta = 88$ (——); $\eta = 220$ (·····); $u_{\text{fe}}(t)$ (——)

is noticeable that for low η ($\eta = 0$ and $\eta = 44$), the results are strongly different from the finite element solution. In comparison, for similar ϕ, the CCM reduced-order models lead to better results. However, while η and ϕ

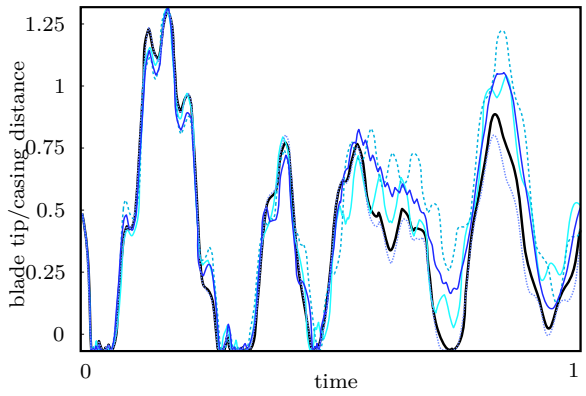

(a) Damped motion, blade 10

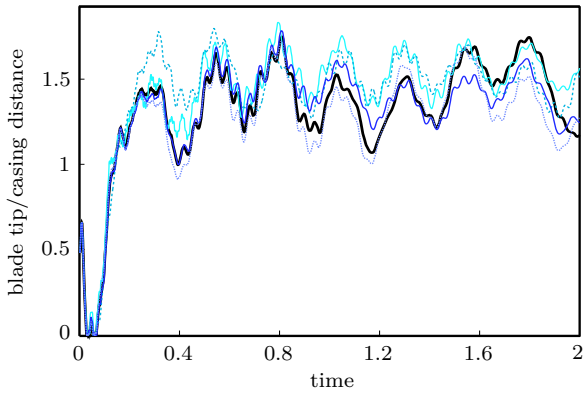

(b) Locked motion, blade 9

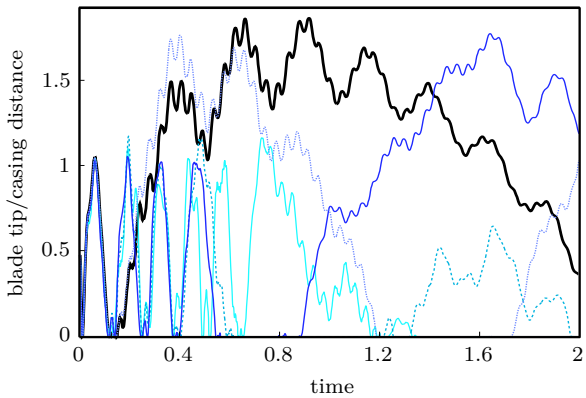

(c) Sustained motion, blade 2

Figure 5 – Convergence of the results obtained with CCM method for each kind of interaction $\phi = 0$ (——); $\phi = 44$ (- - -); $\phi = 88$ (——); $\phi = 220$ (·····); $u_{\text{fe}}(t)$ (——)

increase, convergence is observed more rapidly for the CB method than for the CCM method as it can be seen in Fig. 6 for a sustained motion.

For both methods, $\eta = 88$ and $\phi = 88$ seem to be the minimum threshold

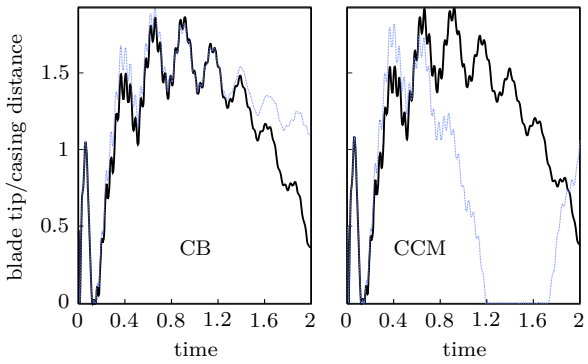

Figure 6 – Comparison of CB (CB) and CCM results (·····) to the finite element solution (——) with $\eta = 220$ and $\phi = 220$

to get good results at the exception of the locked motion with CB reduced-order models $\eta = 88$ is a lower bound. Comparatively to the total number of dof of the bladed disk, these values of η and ϕ may appear very high ($\simeq$ 12%). Such a ratio might not be acceptable in the case of complex industrial 3D models containing several millions of dof. Consequently, it is of interest to ensure that *displacement convergence* requires higher η and ϕ than *motion convergence* in terms of type of detected motions.

Motion convergence

In order to assess the convergence in terms of motions, reduced-order models are built with $\eta = 44$, $\eta = 88$, $\phi = 44$ and $\phi = 88$. Several simulations are performed while increasing the rotational velocity Ω and friction coefficient μ. Resulting maps, illustrated in Figs. 7 and 8 allow for an estimation of the influence of detected motions to parameters η and ϕ for $n_d = 2$. Areas in black (■) represent divergent motions, areas in grey (▬) represent locked motions and white areas show damped motions. The comparisons displayed in Figs. 7 and 8 suggest that motion convergence is easily reached with the CB method. For both CB and CCM reduced-order models, it can be observed that a smaller modal description ($\eta = 44$ and $\phi = 44$) tends to favor damped motions. In the specific case of the CB reduced-order model, the value of η does not disturb the transition between the locked motion and the divergent motion areas. However, for CCM reduced-order models, this transition is modified and the locked motion area is less homogeneous for $\phi = 44$.

The results for the CCM reduced-order models put into perspective the results pictured in Figs. 5(a), 5(b) and 5(c) emphasizing the importance of a large ϕ to reach motion convergence. Only a few differences are distinguishable between the maps for $\eta = \phi = 88$, particularly for low rotating speeds and low friction coefficients. The fact that these two maps match – and because they are obtained with two different CMS methods using dif-

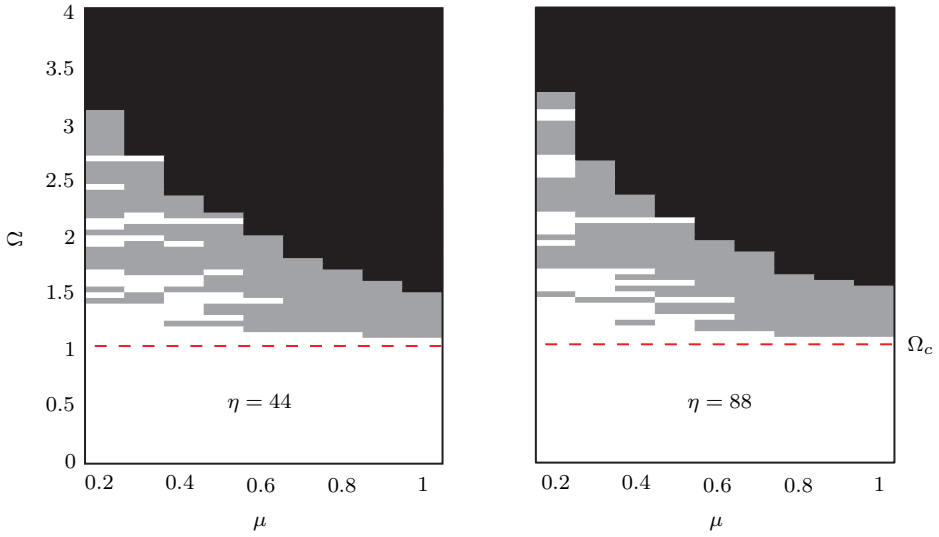

Figure 7 – Motions detected with CB method for $\eta = 44$ and $\eta = 88$ function of μ and Ω

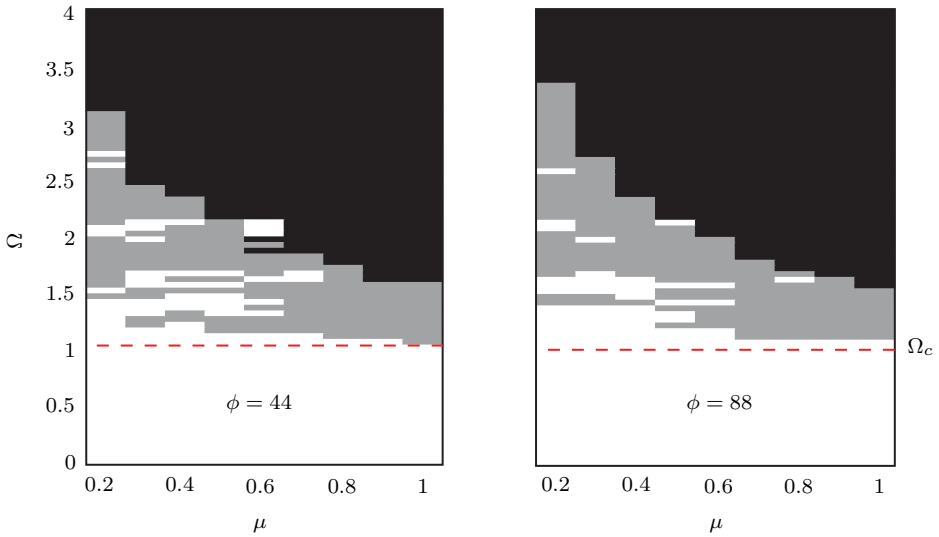

Figure 8 – Motions detected with CCM method for $\phi = 44$ and $\phi = 88$ function of μ and Ω

ferent reduction basis – justifies that results converged in terms of motions. A similar map with finite element models cannot be obtained since it would lead to prohibitive computation times.

5 Conclusions

The combination of component mode synthesis methods with a contact algorithm based on the Lagrange multiplier technique was introduced in [10, 19]. Our study shows that the use of a CMS method minimizes computation times depending the type of convergence sought. For planar finite element models, it was shown that a reasonable number of modes in the modal reduction basis – such as $\eta = 44$ in CB method – are necessary to precisely determine the different motions. However, in order to get a good accuracy in terms of displacements, the size of the modal reduction basis has to be increased due to the high numerical sensitivity of the locking phenomenon. In that case, CCM gives better results with a smaller reduction basis.

Considering these results, work is in progress to evaluate the influence of the kinematic restrictions used in our study on the casing and their role in modal interaction detection.

Acknowledgment

Thanks go to Snecma for its technical and financial support. This work takes place in the framework of the MAIA mechanical research and technology program sponsored by CNRS, ONERA and SAFRAN Group.

References

[1] Legrand, M., 2005. "Modèles de prediction de l'interaction rotor/stator dans un moteur d'avion". Phd thesis, École Centrale de Nantes, Nantes, France.

[2] Legrand, M., Pierre, C., Cartraud, P., and Lombard, J. P., 2009. "Two-dimensional modeling of an aircraft engine structural bladed disk-casing modal interaction". *Journal of Sound and Vibration,* **319**(1-2), pp. 366–391.

[3] Schmiechen, P., 1997. "Travelling wave speed coincidence". Phd thesis, Imperial College of London.

[4] Berthillier, M., and Mascarell, J. P. Vibration des roues aubagées : étude de l'interaction rotor-stator, rapport interne ylec n dr/152/91. Tech. rep., Snecma.

[5] Rixen, D. J., 2004. "A dual craig-bampton method for dynamic substructuring". *Journal of Computational and applied mathematics,* **168**, pp. 383–391.

[6] Craig, R. R. J., and Bampton, M. C. C., 1968. "Coupling of substructures for dynamic analyses". *AIAA Journal,* **6**(7), pp. 1314–1319.

[7] Craig, R. R. J., 1977. "Methods of component mode synthesis.". *Shock and Vibration Digest Journal,* **9**, pp. 3–10.

[8] Tran, D. M., 2000. "Component mode synthesis methods using interface modes. application to structures with cyclic symmetry". *Computers & Structures,* **79**, pp. 209–222.

[9] Martinez, D. R., Carne, T. G., Gregory, D. L., and Miller, A. K., 1984. "Combined experimental/analytical modeling using component mode synthesis". *Computers & Structures,* **78**, pp. 583–590.

[10] Batailly, A., Legrand, M., Cartraud, P., Pierre, C., and Lombard, J. P. "Study of component mode synthesis methods in a rotor-stator interaction case". Proceedings of the ASME 2007 International Design Engineering Technical Conferences & Computers and Information in Engineering Conference: IDETC07, September 2007, Las Vegas, Nevada.

[11] Swaminathan, M., and Rao, J. S., 1977. "Vibrations of rotating, pretwisted and tapered blades". *Mechanism and Machine Theory,* **12**, pp. 331–337.

[12] Kuang, J. H., and Huang, B. W., 1999. "Mode localization of a cracked blade disk". *Journal of Engineering for Gas Turbines and Power,* **121**, pp. 335–341.

[13] Young, T. H., 1991. "Dynamic response of a pretwisted, tapered beam with non-constant rotating speed". *Journal of Sound and vibration,* **150**, pp. 435–446.

[14] Raveendranath, P., Singh, G., and Pradhan, B., 2000. "Free vibration of arches using beam element based on a coupled polynomial displacement field". *Journal of Computational and applied mathematics,* **168**, pp. 383–391.

[15] Simo, J. C., and Laursen, T. A., 1992. "An augmented lagrangian treatment of contact problems involving friction". *Computers & Structures,* **42**(1), pp. 97–116.

[16] Carpenter, N., Taylor, R., and Katona, M., 1991. "Lagrange constraints for transcient finite element surface contact". *International Journal for Numerical Methods in Engineering,* **32**, pp. 103–128.

[17] Tournour, M. A., Atalla, N., Chiello, O., and Sgard, F., 2001. "Validation, performance, convergence and application of free interface component mode synthesis". *Computers & Structures,* **79**, pp. 1861–1876.

[18] Craig, R. R. J., and Chang, C. J. "On the use of attachment modes in substructure coupling for dynamic analysis". presented at AIAA/ASME

18th Structures, Structural Dynamics and Materials Conference, San Diego, California.

[19] Batailly, A., 2008. "Simulation de l'interaction rotor/stator pour des turbomachines aéronautiques en configuration non-accidentelle". Phd thesis, École Centrale de Nantes, Nantes, France.